적층보의 박리좌굴에 관한 해석적 연구

Analytical Study of Delamination Buckling in Laminated Beams

김 영 찬[1)]
KIM, Young Chan

ABSTRACT : 연직하중을 받는 적층보에서 박리좌굴하중을 산정하는 방법을 제시하였다. 재료역학적 방법에 근거하여 박리된 보의 변위함수를 설정하였으며 힘과 변위의 적합조건을 이용하여 연직하중과 박리좌굴하중과의 관계식을 유도하였다. 또한 박리의 진전을 판단하기 위한 변형도에너지 방출율(release rate)을 산정하였다. FRP로 보강된 GLULAM보에 대한 실험과 비교한 이론해는 정확한 결과를 보여 주었으며 연직하중을 받는 적층보의 박리 진전현상은 축하중을 받는 보와는 다른 거동을 보였다.

1. Introduction

Delamination in laminated structures is a separation of adjoining layers at the interface. Delamination growth may significantly influence the strength, stiffness, and stability of a laminate. The initiation of delamination results from many sources, such as manufacturing defects, deterioration of bonding materials, or local impact damage. The delamination behavior in laminated structures has received the attention of several investigators. Basically, most of the available analytical and numerical solutions assumed an embedded delamination before loading and no delamination propagation.

One of the first analytical delamination models was developed by Chai.[1] He characterized the delamination in homogeneous, isotropic plates using a thin-film model, and extended this approach to a general bending case which included the bending of a thick base laminate. Tracy and Pardoen[2] studied the effect of delamination on the flexural stiffness of laminated beams, but their analytical solution did not include bending-extension coupling nor delamination buckling. They tested specimens manufactured with a delamination at the midplane, and they concluded that the delamination did not degrade much the stiffness of the laminates. However, as observed in glulam-FRP beam tests (Kim[3]), if the delami-

1) 대림산업 기술연구소, 선임연구원, 공학박사

nation was placed near the top surface of a beam, delamination buckling is likely to occur. Consequently, the stiffness of the beam would be affected substantially. Currently, there are no studies on the delamination phenomenon in laminated beams under bending.

In this paper, an analytical model to predict the response of a delaminated beam under bending is presented. The investigation of the critical loads and delamination behavior is the major concern of this study. In the analytical model, an initial delamination length at the interface of the top layer and the base laminate is assumed. Beyond the delamination length, the rest of top layer remains bonded to the compression face of a relatively thick laminate. The delaminated beam is subjected to four-point bending and the initial delamination is symmetric about the midspan. The displacement, rotation, and the axial force acting at the delaminated layer are computed, based on the assumed displacement functions which are derived using boundary conditions and compatibility conditions. Also, explicit expressions for critical buckling load and strain energy release rate are provided. Using the test data of a full-size laminated beam, the displacement and critical loads predicted by this study are compared with experimental values. A parametric study is carried out to investigate the effect of laminate stiffness on the critical loads. Strain energy release rate for various initial delamination lengths are computed to find out the trend of delamination growth in laminated beams under bending. Finally, findings of this study are summarized and recommendations for future research are suggested.

2. Derivation of Displacement Functions

Consider the beam shown in Fig. 1 subjected to 4-point symmetric loading, where one half of the beam is modeled using a shear-release at midspan where shear is free but moment is present. The beam is divided into three zones: zone 1 contains no delamination; zone 2 is the base laminate, or thicker lower portion of the delaminated region; and zone 3 is the thin upper lamina that has undergone delamination. The subscripts used in the derivation of the theory correspond to these three zones.

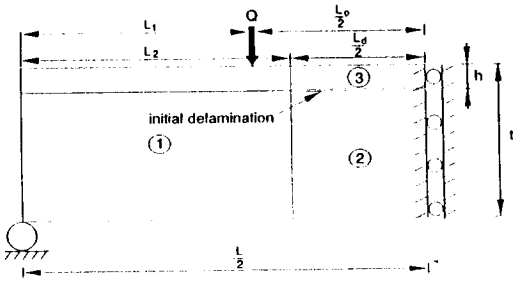

Fig. 1 Beam Configuration and Load

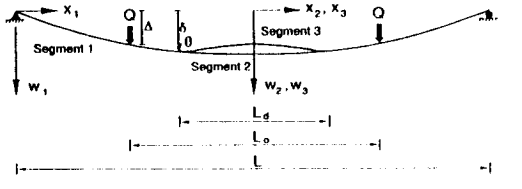

Fig. 2 Coordinate System

The coordinate system and beam parameters are shown in Fig. 2. For the simplification of the problem of interest, we assume that a single delamination is embedded before loading and it is symmetric about the midspan. Also we assume that mode I(opening mode) fracture is the primary mechanism for delamination growth, and that the thickness of a

delaminated lamina is small compared to that of the laminated beam. The displacement functions in all four segments are derived next.

(1) From the support to the loading point

$(0<x_1<L_1)$

As the bending moment varies linearly in this region, the displacement function can be assumed as

$$w_{1a}(x_1) = ax_1^3+bx_1^2+cx_1+d \tag{1}$$

Using the boundary condition at the support and constitutive equation, we have

$$w_{1a}(x_1) = -\frac{Q}{6D_1}x_1^3+cx_1 \tag{2}$$

The coefficient c will be determined in the next section using compatibility conditions.

(2) From the loading point to the delamination tip

$(L_1<x_1<L_2)$

As the bending moment is constant in this region, the displacement function can be written as

$$w_{1b}(x_1) = ex_1^2+fx_1+g \tag{3}$$

Using the constitutive relation and the prescribed boundary conditions at the delamination tip, δ and θ, we obtain

$$w_{1b}(x_1) = \frac{QL_1}{2D_1}(-x_1^2 + 2L_2x_1) + \theta x_1 + \delta - L_2\theta - \frac{QL_1L_2^2}{4D_1} \tag{4}$$

The continuity condition of rotation at $x_1 = L_1$ gives

$$c = \frac{QL_1(2L_2-L_1)}{2D_1}+\theta \tag{5}$$

Then, Eq. (2) becomes

$$w_{1a}(x_1) = -\frac{Q}{6D_1}x_1^3+[\frac{QL_1(2L_2-L_1)}{2D_1}+\theta]x_1 \tag{6}$$

From the displacement continuity condition at $x_1 = L_1$, we have

$$\theta = -\frac{QL_1L_2}{2D_1}+\frac{2QL_1^3}{3D_1L_2}+\frac{\delta}{L_2} \tag{7}$$

(3) Delaminated region: segment 2 $(-\frac{L_d}{2}<x_3<0)$

Assuming a constant bending moment in this region, the displacement function is given by

$$w_2(x_2) = hx_2^2+ix_2+j \tag{8}$$

Using the prescribed boundary conditions at the delamination tip, we have

$$w_2(x_2) = -\frac{\theta}{L_d}x_2^2 + \delta + \frac{\theta}{4}L_d \tag{9}$$

(4) Delaminated region: segment 3 $(-\frac{L_d}{2}<x_3<0)$

The post-buckling deflection shape of a column is given as

$$w_3(x_3) = K_1\sin(\alpha x_3)+K_2\cos(\alpha x_3)+K_3x_3+K_4 \tag{10}$$

where, $\alpha=\sqrt{P/D_3}$. As the deformed shape is

symmetric, we have $K_1 = K_3 = 0$. Using the compatibility of displacement δ and rotation θ at the interface between segments 1 and 3, Eq. (10) becomes

$$w_3(x_3) = \frac{\cos(\alpha x_3) - \cos\beta}{\alpha \sin\beta}\theta + \delta \qquad (11)$$

Where, $\beta = \alpha L_d/2$. The displacement functions expressed in terms of beam parameters and the prescribed boundary conditions are used to compute strain energy and strain energy release rate in a beam, as discussed next.

3. Critical Buckling Load and Delamination Growth

Beam bending induces a strain distribution that is linear through the thickness of the beam. The linear strain distribution can be represented by resultant moments for segments 1 and 2 and resultant axial force acting at segment 2, as shown in Fig. 3. From the moment equilibrium condition at the delamination tip ($x = L_2$), we can write

$$M_1 = M_2 + \frac{Pt}{2} \qquad (12)$$

Using the moment-curvature relations of M_1 and M_2, and the second derivatives of (4) and (9), we have

$$M_1 = -D_1 \frac{d^2 w_1}{dx_1^2} = QL_1$$

$$M_2 = -D_2 \frac{d^2 w_2}{dx_2^2} = \frac{2D_2\theta}{L_d} \qquad (13)$$

Using Eqs. (12) and (13), θ can be expressed as

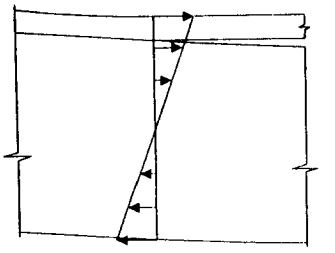

Strain Distribution

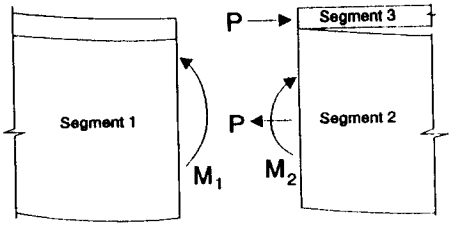

Resultant Forces

Fig. 3 Forces at Delamination Tip

$$\theta = \frac{L_d}{4D_2}(2QL_1 - Pt) \qquad (14)$$

The compatibility condition of axial shortening of segments 2 and 3 is

$$\frac{P}{A_3}L_d = \frac{1}{2}\int_{\frac{-L_d}{2}}^{\frac{L_d}{2}} \left(\frac{dw_2}{dx_2}\right)^2 dx_2 + t\theta - \frac{P}{A_2}L_d \qquad (15)$$

Then, we obtain

$$\theta = -\frac{3t}{L_d} + \sqrt{\frac{9t^2}{L_d^2} + 6\left(\frac{1}{A_2} + \frac{1}{A_3}\right)P} \qquad (16)$$

Equating expressions (14) and (16), the relation between P and Q is established as

$$Q = \frac{2Pt}{L_1} - \frac{8D_2}{L_d L_1} \times \left[\frac{3t}{L_d} - \sqrt{\frac{9t^2}{L_d^2} + 6P\left(\frac{1}{A_2} + \frac{1}{A_3}\right)}\right] \qquad (17)$$

Using the displacement functions given in Eqs. (4), (6), (9), and (11), the strain energy along the post-buckling path for each segment is computed as follows. First, the bending energy for segment 1 is

$$U_1 = \frac{1}{2} D_1 \int_0^{L_2} \left(\frac{d^2 w_1}{dx_2}\right)^2 dx = \frac{(L_1)^2(L+2L_0-3L_d)}{12D_1} Q^2 \tag{18}$$

The bending energy for segment 2 is

$$U_2 = \frac{1}{2} D_2 \int_0^{\frac{L_d}{2}} \left(\frac{d^2 w_2}{dx^2}\right)^2 dx = \frac{L_d}{16D_2}(2QL_1 - P_{cr}t)^2 \tag{19}$$

and the membrane and bending energy for segment 3 is

$$U_3 = \frac{1}{2}\varepsilon_{cr}^2 A_3 \frac{L_d}{2} + \frac{1}{2} D_3 \int_0^{\frac{L_d}{2}} \left(\frac{d^2 w_3}{dx^2}\right)^2 dx = \frac{P_{cr}^2 L_d}{4A_3} + \frac{P_{cr}\theta^2}{8\sin^2\beta_{cr}}\left(L_d + \sin 2\beta_{cr}\sqrt{\frac{D_3}{P_{cr}}}\right) \tag{20}$$

The total potential energy can be written as

$$\Pi = U_1 + U_2 + U_3 - Q\Delta \tag{21}$$

where, Δ, the displacement at a loading point computed using Eq. (6), is

$$\Delta = \theta L_1 + \frac{Q(L_1)^2(L+2L_0-3L_d)}{6D_1} \tag{22}$$

The total potential energy along the post-buckling path can be expressed in terms of a single parameter (Q) as

$$\Pi = \frac{1}{16}\frac{L_d(2QL_1 - P_{cr}t)^2}{D_2} + \frac{1}{64}\frac{P_{cr}L_d^2(2QL_1 - P_{cr}t)^2}{D_2^2[1-\cos(2\beta_{cr})]} \times \left[L_d + \sin(2\beta_{cr})\sqrt{\frac{D_3}{P_{cr}}}\right] + \frac{P_{cr}^2 L_d}{4A_3} - \frac{QL_dL_1}{4D_2}(2QL_1 - P_{cr}t) - \frac{Q^2(L_1)^2(L+2L_0-3L_d)}{12D_1} \tag{23}$$

Then, the critical buckling load (bifurcation point) can be found as (Timoshenko and Gere[4]; Ziegler,[5] Eq. (1.36), p.11)

$$\frac{\partial \Pi}{\partial Q} = 0 \tag{24}$$

or

$$\frac{3}{4}\frac{P_{cr}L_d^2(2QL_1 - P_{cr}t)}{D_2^2 \sin^2\beta_{cr} L_1}\left(L_d + \sqrt{\frac{D_3}{P_{cr}}}\sin 2\beta_{cr}\right) - \left(\frac{L+2L_0-3L_d}{D_1} + \frac{3L_d}{D_2}\right)Q = 0 \tag{25}$$

At the bifurcation point, the load Q in Eq. (17) can be substituted into Eq. (25). Then, P_{cr} is found by an iterative numerical method. Then, substituting P_{cr} into Eq. (17), a critical transverse load Q_{cr} can be computed and it is valid up to the critical stage. Note that in Eq. (20), the load in the delaminated segment is assumed to remain constant and equal to P_{cr}. This is because of the virtually flat post-buckling path, similar to that of an Euler column.

The strain energy release rate (G) is defined as

$$G = -\frac{\partial(U_1+U_2+U_3)}{\partial L_d} \tag{26}$$

and using Eqs. (13) through (20), the explicit expression of G per unit width is

$$G = \frac{(L_1)^2Q^2}{2bD_1} - \frac{(2QL_1 - P_{cr}t)^2}{8bD_2}$$

$$- \frac{P_{cr}L_d^2(2QL_1 - P_{cr}t)^2}{64bD_2^2\sin^2\beta_{cr}}\left(2 - \sqrt{\frac{P_{cr}}{D_3}}\frac{L_d}{\tan\beta_{cr}}\right) \quad (27)$$

The accuracy of the model developed in this section is evaluated by correlating the analytical solutions with experimental results, as presented next.

4. NUMERICAL EXAMPLE

The test data for glulam beams reinforced with GFRP (Kim[3]) are used to validate the analytical solution presented previously. The beam configuration and average layer material properties are shown in Fig. 4, and the beam parameters are listed in Table 1. The delaminated length (L_d), which is unknown at the time of the test, is a parameter needed to carry out the computations with the equations derived in the previous section. The delaminated length is estimated using Lamination Beam Theory (LBT, Barbero[6]) and Euler's column buckling formula. The critical experimental load $Q_{cr}^{exp}=47.2KN$ was recorded when buckling of the delaminated layer was observed during the experiment (see Fig. 5). Using LBT, the stress in the delaminated layer at buckling (bifurcation point) can be computed using the known critical load Q_{cr}^{exp} as follows:

$$\sigma_{cr} = \frac{ME_iy_i}{D_1} = \frac{Q_{cr}^{exp}L_1E_iy_i}{D_1} = 82\ (KN) \quad (28)$$

Table 1. Beam Parameters

Length(m)	L=5.79, L_0=1.83
Axial Stiffness(MN m^2)	A_2=428.8, A_3=20.1
Bending Stiffness(GN m^2)	D_1=7.96, D_2=7.03, D_3=5.87
Thickness(cm)	h=0.48, t=33.9
Width(cm)	b=10.15

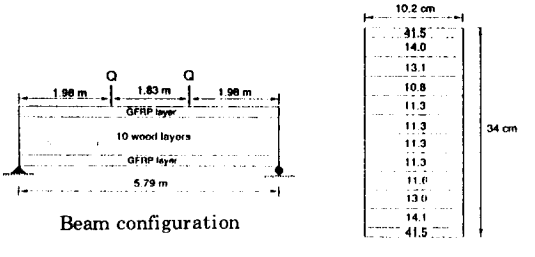

Fig. 4 Laminated Beam Reinforced with GFRP

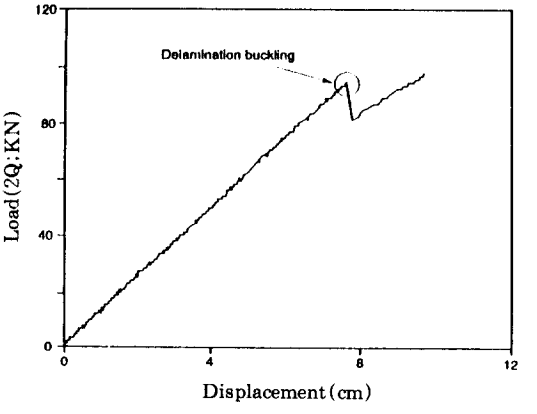

Fig. 5 Load-Deflection Curve

Assuming that the delaminated layer behaves like a fixed-fixed column, the approximate delamination length is computed from Euler's formula as

$$L_d = \sqrt{\frac{4D_3\pi^2}{\sigma_{cr}hb}} = 0.16\ (m) \quad (29)$$

Using Eqs. (17) and (16), P and θ can be computed for a given Q. Then, the maximum midspan deflection w_{2max} is given by Eq.(9) as

$$w_{2max} = \delta + \frac{\theta}{4} L_d \tag{30}$$

The internal axial force P_{cr} in the delaminated lamina and the critical transverse load Q_{cr} are related by Eq. (17). It is our interest to predict Q_{cr} which causes local buckling of a delaminated sublaminate. In Fig. 6, P_{cr} and Q_{cr} are plotted for various delamination lengths, where P_{cr} is computed from Eq. (27) and Euler's formula, and Q_{cr} is obtained from Eq. (17). Euler's formula and the results of Eq. (27) provide nearly identical values for P_{cr}. However, Euler's formula can not by itself provide any information on the magnitude of the transverse load (Q). Therefore, Eq. (17) must be used. The experimental load-displacement path of the glulam-GFRP beam is given in Fig. 5, and the experimental values and analytical solutions are compared in Table 2. Compared

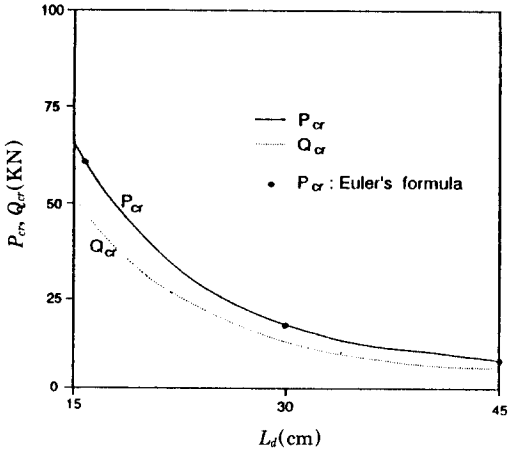

Fig. 6 Critical Loads

Table 2. Comparison of critical loads

Q_{cr}(KN)		P_{cr}(KN)	
Test	This study	Test	This Study
47.2	48.5	61.9	61.4

with test results, the critical load Q_{cr} predicted by this study is within 2.6% of the experimental value, and the predicted P_{cr} is within 1% of the experimental P_{cr}. The experimental P_{cr} is computed using the experimental strain at the top surface measured with strain gages.

After the buckling of a delaminated sublaminate occurs, it is of interest to investigate the growth of the delamination length; i. e., whether or not the delamination will grow or be arrested as function of the applied load. For this purpose, the strain energy release rate given in Eq. (27) is plotted for various initial delamination lengths in Fig. 7. To interpret the physical meaning of the curves, a critical strain energy release rate (G_{Ic}) is assumed as 87.6 (N/m). This value of G_{Ic} is representative of graphite-epoxy T300/976. When the transverse load reaches a critical value (Q_{cr}=48.5KN for the example considered in this study), the delamination becomes unstable, and it grows from the initial delamination length (L_d=0.

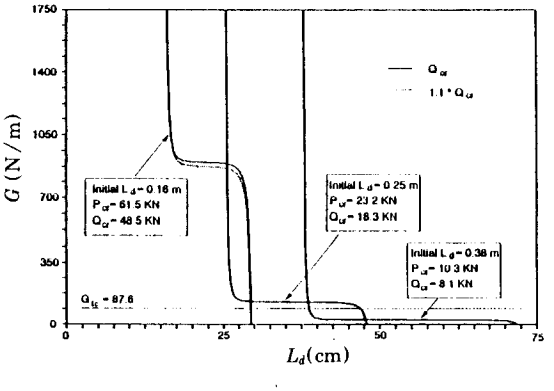

Fig. 7 Strain Energy Release Rate Curves

16m) to a stable condition (L_d=0.3m). Increasing the load by a factor of 10% of Q_{cr}, the delamination length decreases slightly, which means that no further delamination growth occurs: i. e., the delamination growth is arrested.

For an initial delamination length of 0.25m, the flat zone of the curve moves down, but the curve is still above the assumed G_{Ic} value, which indicates an unstable delamination growth in the beam, leading to a stable condition at the delamination length of around 0. 48m. However in this case, Q_{cr} decreases by 60% to a value of 18.3KN, when compared to the previous case for L_d=0.16m. For a further increase of delamination length to 0.38m, the flat zone of the curve moves below the assumed G_{Ic} value, and therefore, there is no delamination growth. Compared to the initial case (L_d=0.16m), Q_{cr} in this case decreases by 80% to a value of 8.1KN. From this observation, we may infer that delamination growth in a thin layer on the compression face of a beam is arrested, while in laminates under axial load the delamination growth can grow indefinitely. Additional experimental data are needed to corroborate this observation.

5. CONCLUSION

Most of the existing studies on delamination in laminated structures deal with an axial loading, irrespective of whether a thin-film model or a general bending model is used. However,the existing models can not be directly applied to a transverse load case, in which the major concern is to find a critical transverse load. The main findings of this study are:

(1) an explicit form to relate the transverse load (Q) with the internal axial force (P) is established.

(2) the critical load (Q_{cr}) can be accurately predicted as corroborated by experiment.

(3) a simulated delamination phenomenon indicates an unstable delamination growth after buckling of the delaminated sublaminate, followed by arrested delamination growth. This response is different from the axial loading case, for which unbounded delamination growth is generally predicted.

To further verify the present model, it is desirable to conduct well-controlled tests of laminated beams with embedded predetermined delamination lengths and instrumented with transducers to detect onset of delamination buckling and measure delamination growth.

REFERENCES

1. Chai, H., 'The growth of impact damage in compressively load laminates'. Ph. D. dissertation, California Institute of Technology, Pasadena, CA, 1982.
2. Tracy, J. J. and Pardoen, G. C., 'Effect of delamination on the flexural stiffness of composite laminates'. Thin-Walled Structures., 6, 371-383, 1988.
3. Kim, Y., 'A layer-wise theory for linear and failure analysis of laminated composite beams'. Ph.D. dissertation, West Virginia University, Morgantown, WV, 1995.
4. Timoshenko, S. P and Gere, J. M., Theory of elastic stability, 2nd ed. McGraw-Hill, New York, 1961.
5. Ziegler, H., Principles of structural stability, Blaisdell Publishing Co., Massachusetts, 1968.
6. Barbero, E. J., 'Pultruded structural shapes-From the constituents to the structural behavior'. SAMPE Journal, 27(1), 25-30, 1991.